Library Progress International
Vol.43 No. 2, Jul-Dec 2023: P. 3067-3081

Print version ISSN 0970 1052
Online version ISSN 2320 317X

Original Article

Available online at www.bpasjournals.com

Synthesis and photocatalytic evaluation of visible Light-Activated (Fe,S)codopedTiO₂ in Metanil yellow degradation

S. Cathaline Jagha

Scholar, (Reg.No.20123112032016), Department of Chemistry and Research, Nesamony Memorial Christian College, Marthandam (Affiliated to Manonmaniam Sundaranar University, Abishekapatti, Tirunelveli), Tamilnadu, India.

E. K. Kirupa Vasam

Assistant Professor, Department of Chemistry and Research, Nesamony Memorial Christian College, Marthandam (Affiliated to Manonmaniam Sundaranar University, Abishekapatti, Tirunelveli), Tamilnadu, India.

How to cite this article: S. Cathaline Jagha, E. K. Kirupa Vasam. (2023) Synthesis and photocatalytic evaluation of visible Light-Activated (Fe,S)codopedTiO₂ in Metanil yellow degradation. *Library Progress International,* 43(2), 3067-3081

Abstract

In this study, visible-light-active **(Fe, S)-codopedTiO₂** photocatalysts were synthesized via a sol–gel method using titanium tetraisopropoxide (TTIP) as the precursor. The structural, optical, morphological, and elemental characteristics of the synthesized photocatalysts were comprehensively analyzed using XRD, FT-IR, SEM–EDX, HR-TEM, and UV–Vis DRS techniques. Metanil Yellow (MY), an azo dye, was selected as a model pollutant to evaluate the photocatalytic efficiency of the synthesized **(Fe, S)-codopedTiO₂** photocatalyst under visible-light irradiation. The results revealed that the **(Fe, S)-codopedTiO₂** photocatalyst (150mg/100 mL) completely degraded MY (20 ppm) within 30 minutes under visible-light exposure. Furthermore, Chemical Oxygen Demand (COD) and Total Organic Carbon (TOC) analyses confirmed a 99% mineralization efficiency. The degradation reaction followed pseudo-first-order kinetics with an apparent rate constant of 0.051×10^{-3} min^{-1} ($R^2 = 0.978$). The photocatalyst exhibited excellent stability and reusability, maintaining high degradation efficiency over five consecutive cycles without significant loss of activity. The enhanced photocatalytic performance of the **(Fe, S)-codopedTiO₂** is attributed to the effective suppression of electron–hole recombination and improved visible-light absorption. The synthesized nanoparticles were stable, well-crystallized, and environmentally benign, making them suitable for the treatment of organic pollutants in industrial and agricultural wastewater under sunlight. Therefore, the fabricated **(Fe, S)-codopedTiO₂** photocatalyst is demonstrated to be an efficient and cost-effective material, as only a small amount of photocatalyst is required for environmental remediation applications.

INTRODUCTION

Water is a basic requirement for everyone's life. The major worldwide challenge for the twenty-first century is to furnish and ensure safe water for the entire ecosystem. Water pollution can be caused by a variety of factors, including agricultural runoff from pesticides and fertilizers, waste water discharged directly into rivers or streams, and other activities [1]. At present, water pollution caused by dyes is a critical issue. Due leaching, runoff, and drifting of these harmful chemicals in water systems cause toxic

effects on aquatic and other living organisms. These toxic chemicals are transported over long distances together with wastewater and remain in the water and soil for long periods, posing serious health risks to living organisms, reducing soil fertility, and affecting the photosynthetic activity of aquatic plants, which can result in anoxic conditions for aquatic fauna and flora [2].

Hence, it is vital to remove such dyes from industrial wastewater before it is discharged into natural water bodies [3]. Conventional water treatment technologies, such as adsorption, coagulation, sedimentation, filtration, and chemical and membrane-based approaches, are often insufficient for complete dye degradation [4, 5]. Therefore, advanced oxidation processes (AOPs) are employed to remove soluble dyes. Among these, photocatalysis is a promising technique that uses light and catalysts to accelerate the degradation of organic pollutants [6]. Previous studies indicate that photocatalysis can remove 70–80% of pigments from industrial effluents.

Semiconductor nanomaterials absorb energy greater than their bandgap, which excites electrons from the valence band to the conduction band, generating electron–hole pairs. When a metal oxide nanoparticle is exposed to UV–Vis radiation, electrons are excited to the conduction band and electron-hole pairs are created [9]. The valence band holes react with surface-bound H_2O to produce hydroxyl (•OH) radicals, while the electrons react with oxygen (O_2) molecules to produce superoxide radical anions ($O_2^{\bullet -}$) [7]. These reactive species oxidize organic dyes, degrading them into carbon dioxide (CO_2), water (H_2O), and other mineralized products [11].

MY is selected as a model test pollutant for the present study due to its toxic nature and extensive application in several industrial sectors like textile, leather, shoe polish, wood stain, paper, food, and cosmetics [8]. Exposure to this dye can cause tumors, anemia, intestinal disorders, and contact dermatitis upon direct skin contact [9]. Therefore, it is necessary to treat industrial effluents before discharging into nearby freshwater streams [10]. Many conventional treatment methods are used for treating industrial effluents including physical, chemical and biological processes. However these methods have several limitations. In contrast, semiconductor-mediated photocatalytic mineralisation of effluent serves as a promising technology, as complete mineralisation is possible at room temperature in the presence of very small amount of photocatalyst .

ZnO [15], TiO_2 [16], CuO [17], WO_3 [18], V_2O_5 [19], ZrO_2 [20], Al_2O_3 [21], SnO_2 [11], and NiO [23] are among the metal oxide-based semiconductors recently used in photocatalysis. Among these, TiO_2 is preferred due to its non-toxic nature, and excellent properties such as low resistivity, high thermal and chemical stability, high optical transmittance, and strong photocatalytic activity [24]. However, the photocatalytic efficiency of TiO_2 is limited due to its wide band gap (3.3eV), its UV-light-dependent excitation, and the high recombination rate of electron-hole pairs (e^-/h^+) [12]. To overcome these limitations, co-doping of TiO_2 with metals and/or non-metals has been explored to enhance its solar-light absorption and reduce electron-hole recombination.

According to literature reported, non-metal doping narrows the band gap of TiO_2, allowing it to absorb visible light instead of being restricted to the UV region which significantly improve its photocatalytic activity (Asahi et al. 2014). Shahid [13] reported that 1% Cu/Zr co-doped TiO_2 (CZTO) nanoparticles achieved 92% degradation of methylene blue within 120 minutes under visible light, with an apparent rate constant 4.6 times higher than that of pure TiO_2. Getye B Y et al. demonstrated that a TiO_2/CuO nanocomposite photocatalyst achieved 99% degradation of methylene blue within 90 minutes under visible light, following pseudo-first-order kinetics with good stability and reusability [14]. Sirivallopet al. showed that 5% N and Ag co-doped TiO_2 achieved 98.82% degradation of methylene blue under visible light in 6 hours, with a significant enhancement due to synergistic effect of N and Ag doping

[16]. Faustino E et al. reported that N- and Fe-codopedTiO_2 nanoparticles achieved 92% mineralization of 2,4-dimethylaniline under UV light within 180 minutes; optimal doping of Fe(0.0125% Fe)on TiO_2 has reduced the band gap to 2.82 eV and thus increased the surface area to 84.73 m^2/g, due to the synergistic effect of N and Fe doping [17].N-doped and Cu-doped TiO_2 have been reported for the photodegradation of various dyes ,whereas limited research is available on Cu and N co-doped TiO_2 on dye degradation**,** highlighting the novelty and significance of the present study.

This study focuses on synthesizing undoped TiO_2 and (Fe, S)co-doped TiO_2 photocatalyst via sol-gel method to improve photocatalytic activity. Metal ions such as Cu^{2+}, Ni^{2+}, Co^{3+}, and Fe^{3+} act as charge carriers, while nitrogen doping introduces 2p states above the valence band, narrowing the band gap for visible-light absorption. Cu serves as an electron trap, and N improves hole mobility, reducing electron-hole recombination. Co-doping also generates oxygen vacancies and enhances surface reactivity, resulting in superior photocatalytic activity compared to undoped TiO_2 [18].

The synthesized (Fe, S)-codopedTiO_2 photocatalyst was characterized using UV–DRS, TEM, SEM, XRD, and FT-IR analysis, confirming the successful incorporation of dopants into the TiO_2 lattice. Photocatalytic efficiency was evaluated via the degradation of MY under sunlight, and mineralization was confirmed through COD and TOC analysis. Furthermore, the quality and durability of the (Fe, S)-codopedTiO_2 photocatalyst were confirmed by recycling it over five successive cycles, demonstrating its stability and reusability for environmental remediation applications.

EXPERIMENTAL METHODS

Materials

The chemicals required for the present study includes: Titanium tetraisopropoxide, (TTIP)$Ti[OCH(CH_3)_2]_4$,Urea (NH_2CONH_2), iron (III) nitrate [(Fe (NO3)3 .9H2 O)], and absolute ethanol (C_2H_6O) (99%) purchased from Merck Specialties Pvt Ltd., Mumbai and ISO-Chem Laboratories, Kochi respectively. These chemicals were procured for the fabrication of (Fe, S)-codopedTiO_2 photocatalyst and are used in pristine form. Double-distilled water is used for all the experimental studies. The photocatalytic irradiation were carried out from 11:00 AM to 2:00 PM on sunny days. For this investigation, Metanil yellow ($C_{18}H_{14}N_3NaO_3S$) was chosen as the test pollutant.

Preparation of undoped TiO2 :

10 mL of Titanium (IV) isopropoxide was dissolved in 10 mL of ethanol (C2 H5 OH) with constant stirring for about 10 minutes using a magnetic stirrer. To this above suspension, 10 mL of double distilled water was added dropwise to bring about hydrolysis. This solution was further stirred for two hrs till it was transformed into a gel. The gel was allowed to stand for 24 hrs aging and further, it was calcinated to 400 ºC to get the undoped TiO2.

Preparation of (Fe, S)-codopedTiO_2 nanocomposite:

To synthesize (Fe, S)-codopedTiO_2 nanocomposite, a sol-gel route was employed. A desired amount of undoped TiO2 was added dropwise to a minimum quantity of ethanol (C2 H5 OH) with constant stirring. The precipitation of the corresponding hydroxide was prevented by the addition of nitric acid (HNO3). To the above suspension iron (III) nitrate [(Fe (NO3)3 .9H2 O)] was added and heated to 50˚C. The reaction mixture was magnetically stirred for 3 hours with the addition of thiourea (CH4 N2 S). Finally, 5 ml of double distilled water was added to induce gelation. The gel was dried at 80˚ C for 3 hrs before being calcined in a muffle furnace at 450˚ C for 2 hrs.

The crystalline size and crystalline phase of the synthesized photocatalyst were calculated by

powder XRD Bruker D8 Advance diffractometer using Ni-filtered Cu Kα radiation (λ=1.5406 A˚) as an incident light in 2θ mode over a range of 20 80˚ operated at 40 kV, and 30 mA. The presence of functional groups and the nature of the photocatalyst were identified using FT-IR (AVATAR 370) using a Jasco FTIR-4600. The optical properties were evaluated using DRS analysis (Agilent Cary 5000) with BaSO4 as the reference material. The surface morphology along with its elemental composition was calculated by SEM (FEIQuantaFEG200F) equipped with an Energy Dispersive X-ray (EDS) Spectrophotometer operated at 30kV and HR TEM, (JEOL-2100) with a rising voltage of 200 kV and resolution point 0.194nm.

RESULTS AND DISCUSSION:

X-ray diffraction Studies

Fig. 1 depicts the XRD pattern of the Fe/S/ TiO2 nanocomposite. The diffraction peaks at 2θ values of 25.4º, 48º, 54.7º, and 63.1º are due to the reflections from (1 0 1), (2 0 0), (1 0 5), (2 0 4), (2 2 0) and (2 15) planes. These diffraction peaks correspond with standard JCPDS Card No. 21 1272 and are in close agreement with the anatase phase of the TiO2 structure. The characteristic peaks at 2θ values of 30.15º, 35.42º, 43.11º, 53.51º, 56.99º, 62.64º, 74.67º can be indexed to (220), (311), (400), (422), (511), (440) and (533) planes of cubic crystal system of iron nanoparticles, respectively [19]. The ionic radius of Fe3+ (0.64A) is closer to that of Ti4+ (0.68A), and it can therefore be easily integrated into the TiO2 lattice [20]. The presence of monoclinic sulfur has shown a sharp and strong diffraction peak at 2θ = 28º correlated to the monoclinic structure of sulfur (JCPDS card no: 24-0735). Based on Scherrer's formula, the average crystallite size of the Fe/S/TiO2 nanocomposite was calculated to be 6.5 nm respectively

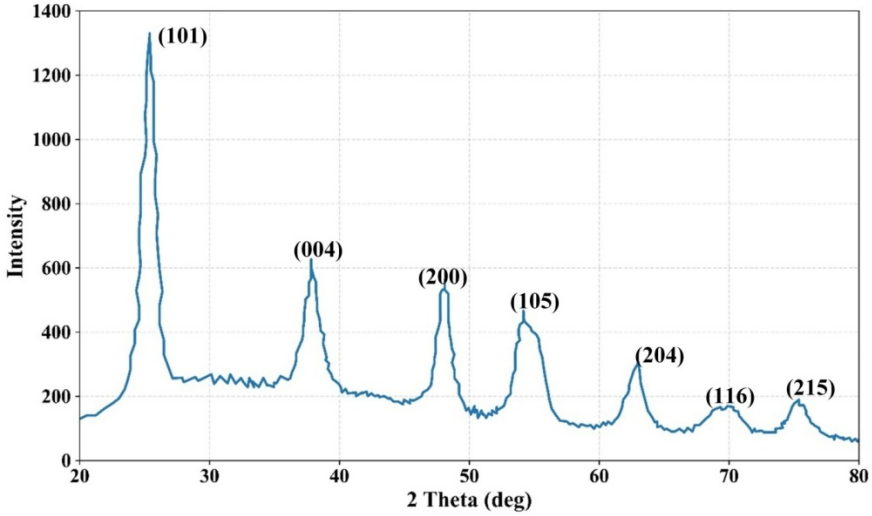

Figure:1 XRD pattern of(Fe, S)-codopedTiO₂

FT-IR Analysis

The vibration bands of the Fe/S/TiO2 nanocomposite were determined by the FT IR analysis, ranging from 500 to 4000 cm-1 as displayed in Fig. 2. In Fe/S/TiO2 nanocomposite, the broad, intense band is located at 1130 cm-1 due to the stretching vibration of Ti-O-Ti linkages in TiO2 nanoparticles which proves the formation of TiO2 [21]. Moreover, the absorption band within the region of 900–1300 cm−1 in Fe/S/TiO2 nanocomposite is a characteristic peak for the formation of the Ti-O-S network. The peak at 1609is assigned due to the surface hydroxylation upon doping TiO2 with Fe. A small peak at 645 cm-1 is. characteristic peak for sulfur [22]. The bands at 3218 cm-1 and 1621 cm-1 correspond to O-H

bending and stretching vibrations of absorbed water molecules respectively, which shows the presence of OH ions in the sample. This may positively contribute to the photocatalytic activity of the synthesized nanocomposite.

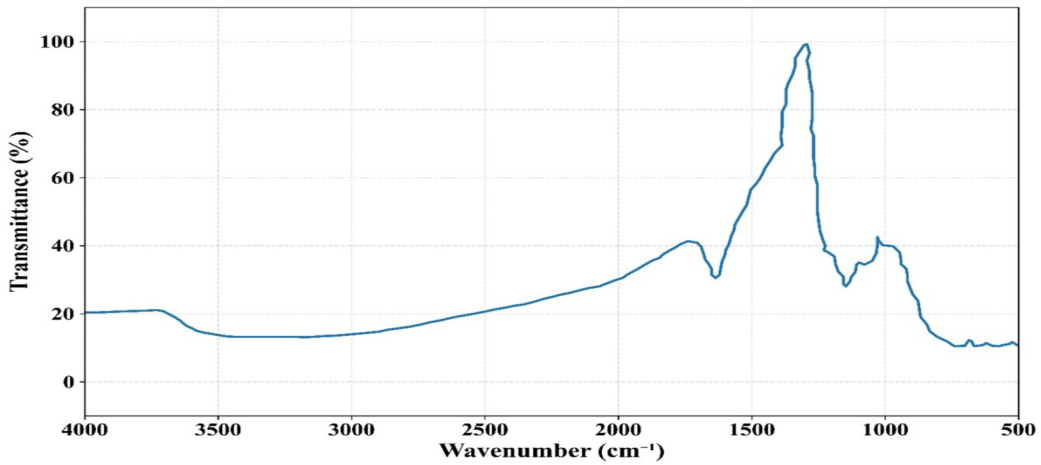

Figure: 2 FTIR structure of(Fe, S)-codopedTiO₂

UV-vis DRS analysis

The optical characteristics of the **(Fe, S) co-doped TiO₂ nanophotocatalyst**were investigated using UV–Vis absorption spectroscopy. The UV–Vis DRS spectra presented in Fig. 4(a), and the corresponding Tauc plot shown in Fig. 4(b), were derived using the Kubelka–Munk function to determine the optical band gap of the synthesized materials. A distinct absorption feature around 297 nm, observed in the Tauc plot, originates from the UV–Vis spectrum and is associated with intrinsic electronic transitions within the TiO_2 lattice. Upon incorporation of Fe and S dopants, a significant shift of the absorption edge toward the longer wavelength region (redshift) was recorded, indicating the narrowing of the band gap and improved light-harvesting ability in the visible region. This enhancement can be attributed to the introduction of impurity energy states by Fe and S, which facilitate electron excitation under lower-energy visible light.The band gap energies for undoped TiO_2 and (Fe–S) codopedTiO_2 were determined to be 3.2 eV and 2.51 eV, respectively, confirming the impact of codoping on modifying the electronic structure of TiO_2. The reduction in band gap is mainly associated with the hybridization of the sulfur p-orbital with the O–2p states of TiO_2 and the interaction of Fe–3d orbitals with Ti–3d orbitals, resulting in the formation of localized defect levels slightly above the valence band [23]. These defect states act as intermediate energy levels that promote efficient charge-transfer processes and suppress electron–hole recombination, thereby enhancing photocatalytic response. Furthermore, Fe dopants can form Fe^{3+}/Fe^{2+} redox pairs, which promote faster electron transfer and enhance charge mobility within the **TiO_2 lattice**. These optical improvements indicate that **(Fe, S) co-doped TiO_2** possesses stronger visible-light absorption, better charge separation, and higher photocatalytic efficiency, making it highly suitable for visible-light-driven environmental purification.

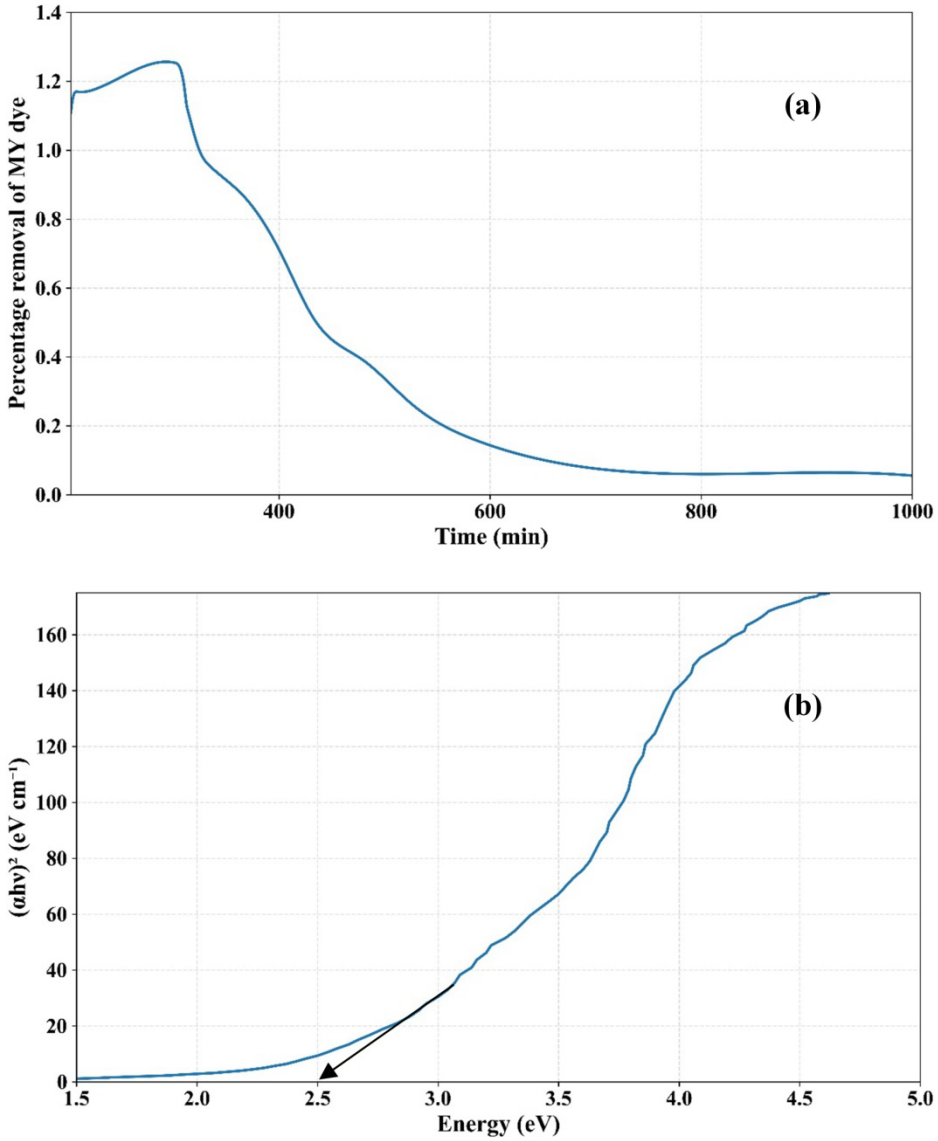

Figure .3 (a) UV -vis diffuse reflectance spectra of **(Fe, S) co-doped TiO_2 (b) Plot of Kubelka -Munk function**

Morphological and elemental analysis

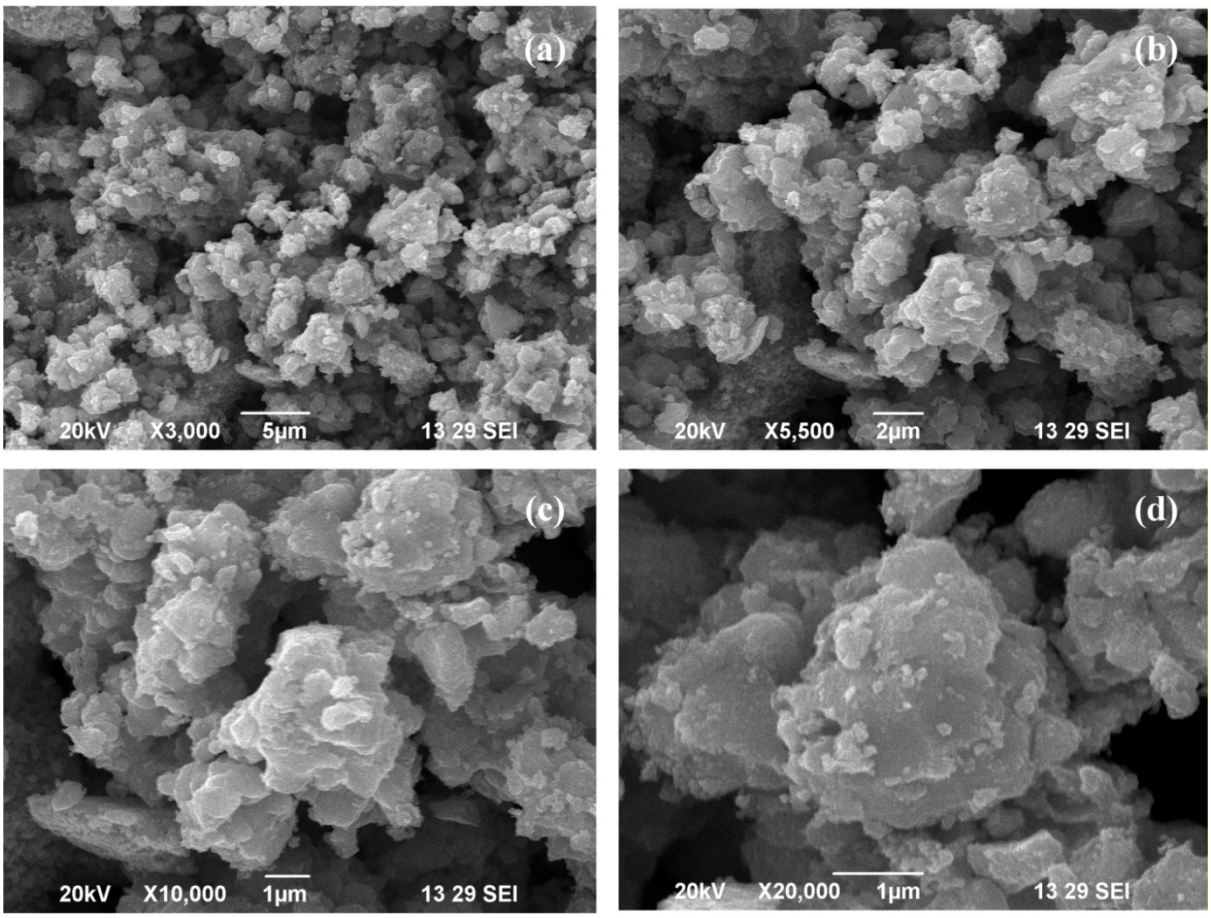

Figure 4:SEM images of(Fe, S)-codopedTiO_2

Figure 4 (a-d) exhibits the SEM images of the constructed samples. The nanocrystals show a fairly similar size, with a large number, thus, a great number of pores have been formed. Most of the particles appear to be highly circular, and the size distribution is uniform [24]. Moreover, Fe and S species have been mixed uniformly.At low magnification (Fig. **a**), the nanoparticles exhibits a **highly agglomerated structure** composed of irregularly shaped particles. This agglomeration is typical for metal oxide–based nanoparticles and mainly arises due to their **high surface energy** and strong interparticle interactions during synthesis and drying processes.With an increase in magnification (Fig. **b**), the morphology becomes clearer, revealing that the agglomerates are formed from **nearly uniform primary nanoparticles** clustered together. The surface appears rough and porous, which is advantageous for photocatalytic reactions as it provides **more active surface sites** for pollutant adsorption.Further magnification (Fig. **c**) shows that the agglomerates consist of **closed packed nanosized grains** with irregular boundaries. The absence of distinct phase separation indicates that the dopant species are well integrated into the TiO_2 matrix rather than forming separate particles.At the highest magnification (Fig. **d**), individual agglomerates display a **rough and heterogeneous surface texture**, confirming the nanocrystalline nature of the material. Such surface roughness and particle clustering can enhance light absorption and charge transfer efficiency, thereby improving photocatalytic performance.Overall, the SEM images confirm the formation of **nanostructured, agglomerated particles with rough surfaces**, which are favorable characteristics for efficient photocatalytic activity.

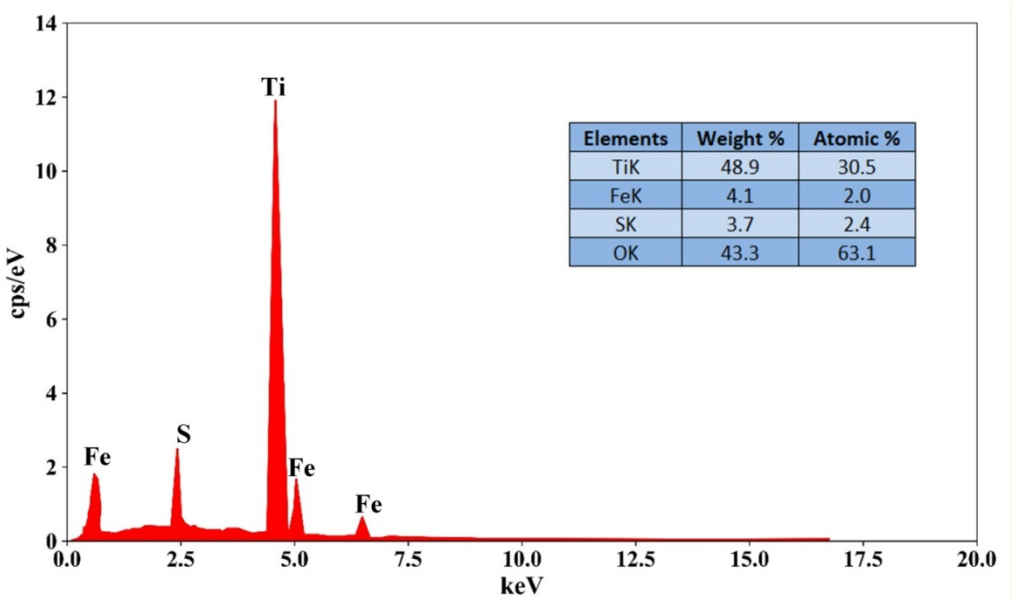

Figure 5:EDAX pattern of(Fe, S)-codopedTiO_2

Elemental analysis using the EDX technique (Fig. 5.5) further validates the formation of (Fe,S)-codopedTiO_2 **nanoparticles**. The spectrum exhibits clear peaks corresponding to titanium (Ti), iron (Fe), sulfur (S), and oxygen (O), demonstrating that the dopants are embedded within the TiO_2 lattice rather than existing as separate elemental phases. No additional peaks were detected, confirming the absence of unwanted metallic impurities. The EDX quantification shows **weight percentages** of approximately **Ti: 48.9 wt%**, **Fe: 4.1 wt%**, **S: 3.7 wt%**, and **O: 43.3 wt%**. The corresponding **atomic percentages** were determined to be **Ti: 32.5 at%**, **Fe: 2.0 at%**, **S: 2.4 at%**, and **O: 63.1 at%**, confirming the successful incorporation of all expected elements into the synthesized nanoparticles.

TEM analysis

Figures 6 (a–d) show the TEM images of the synthesized photocatalyst recorded at different magnifications.**Figure (a)** presents a low-magnification TEM image, revealing that the material is composed of **closely packed nanoparticles forming large agglomerates**. This agglomeration is commonly observed in metal oxide nanoparticles and arises from **strong interparticle interactions and high surface energy** during synthesis and drying.**Figure (b)** provides a clearer view of the aggregated structure. The image confirms that the agglomerates consist of **nearly spherical nanoparticles** with relatively uniform size distribution. The absence of distinct secondary phases suggests **homogeneous composition** within the sample.**Figure (c)** shows individual nanoparticles more distinctly. The particle size is observed to be in the **nanometer range**, and the particles appear to be closely interconnected, forming a porous network. Such morphology is beneficial for photocatalytic applications as it provides **a large surface area and more active sites**.**Figure (d)** represents a high-resolution TEM (HRTEM) image. Clear **lattice fringes** are visible, indicating the **crystalline nature** of the nanoparticles. The presence of well-defined fringes confirms good crystallinity, which plays a important role in **reduced electron–hole recombination** during photocatalysis.

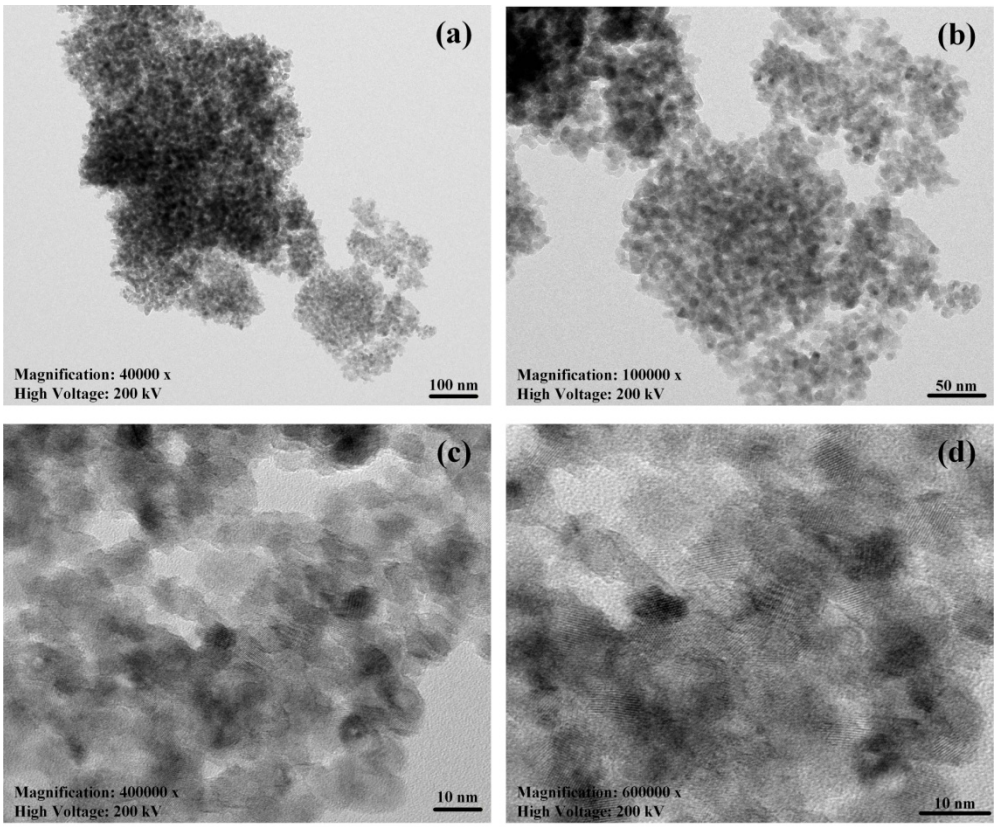

Figure 6:TEM images of(Fe, S)-codopedTiO_2

Particle size distribution histograms, obtained using Gaussian fitting, are shown in Fig. 8(a). Based on these analyses, the average particle size of the (Fe, S)-codopedTiO_2 nanoparticles was calculated to be approximately 6.51 nm. These findings are in good agreement with the results obtained from the XRD pattern. The nanoscale size of the photocatalysts plays a important role in enhancing their electronic, optical, and catalytic properties, thereby contributing to improved photocatalytic performance[25].Particle size distribution from TEM analysis is obtained by measuring the diameters of a large number of individual particles directly from TEM micrographs. The distribution provides information on average particle size, size range, and uniformity of the synthesized material.

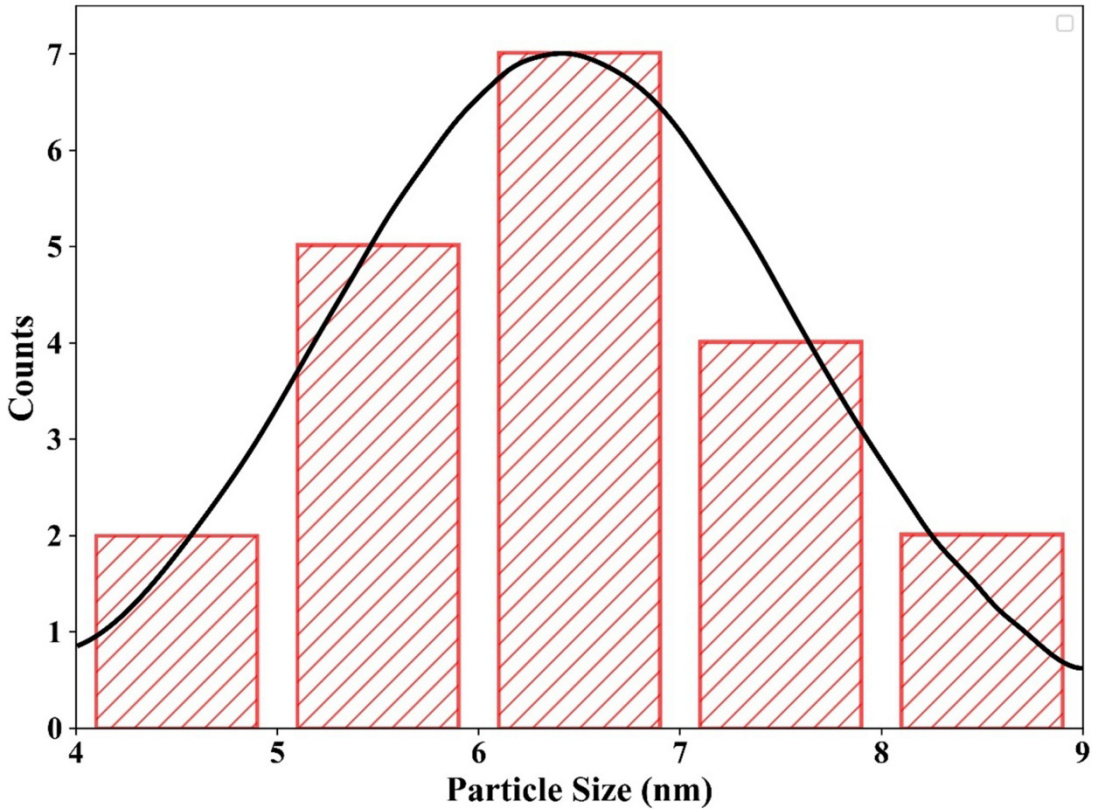

Figure: 7 **Particle size distribution of the** (Fe, S)-codopedTiO$_2$ photo**catalyst**

Photostability and reusability of the (Fe, S)-codopedTiO$_2$ photo**catalyst**

The photostability and reusability of (Fe, S)-codopedTiO$_2$ are important for photocatalytic degradation, as they help reduce operational costs [26] . To check its stability, the catalyst was subjected to eight consecutive photocatalytic cycles under optimized conditions[27]. After each cycle, the used catalyst was collected, thoroughly washed,dried in an oven, and reused in the next experiment. The degradation efficiency of MY dye remained at 100% for the first six cycles and decreased slightly to 96% and 92% in the last two cycles. These results indicate that (Fe, S)-codopedTiO$_2$ exhibits excellent stability and recyclability, confirming its effectiveness as a good photocatalyst for environmental pollutant removal.

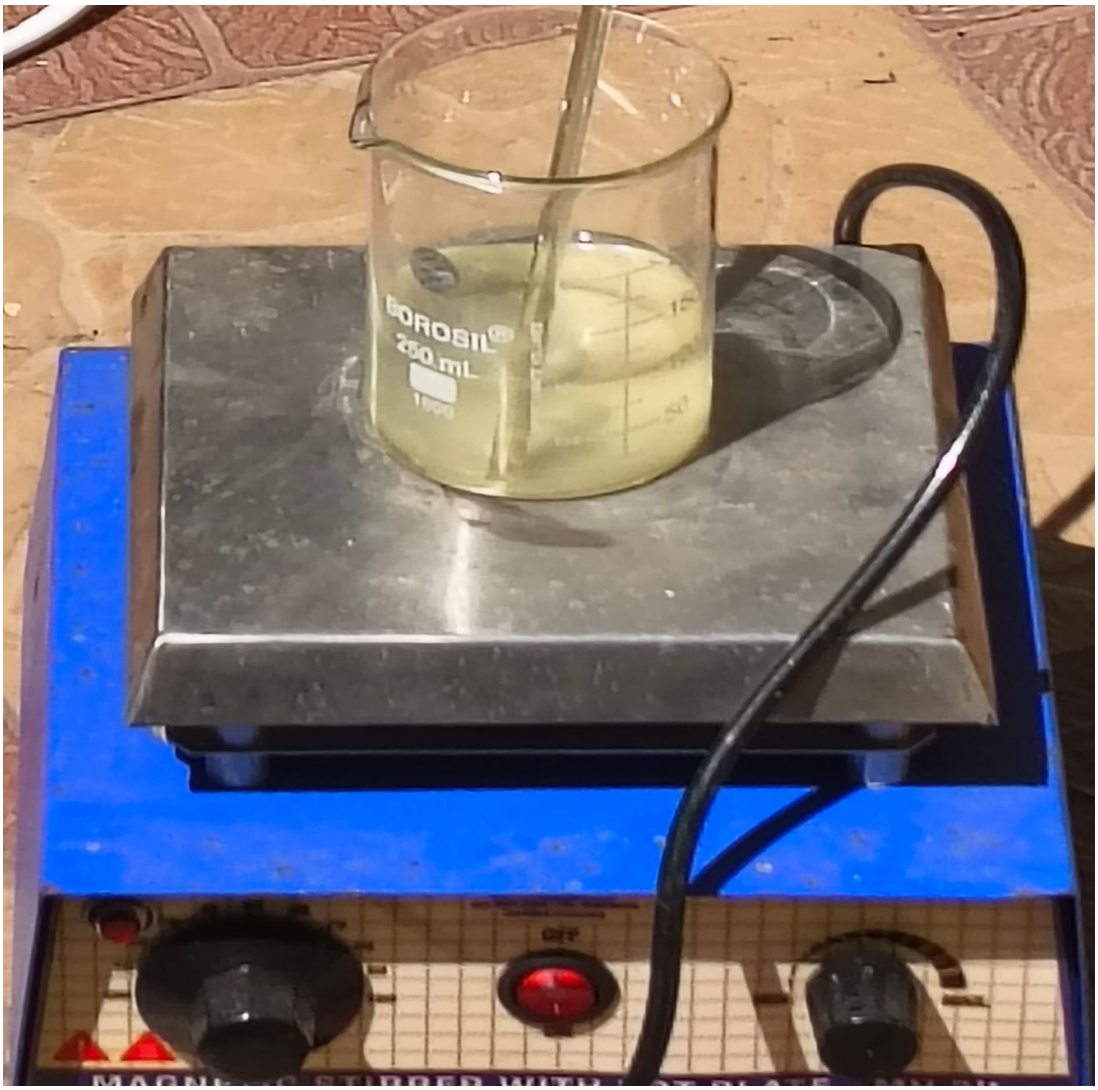

Figure 8. Recycling experiment setup of (Fe, S)-codopedTiO_2

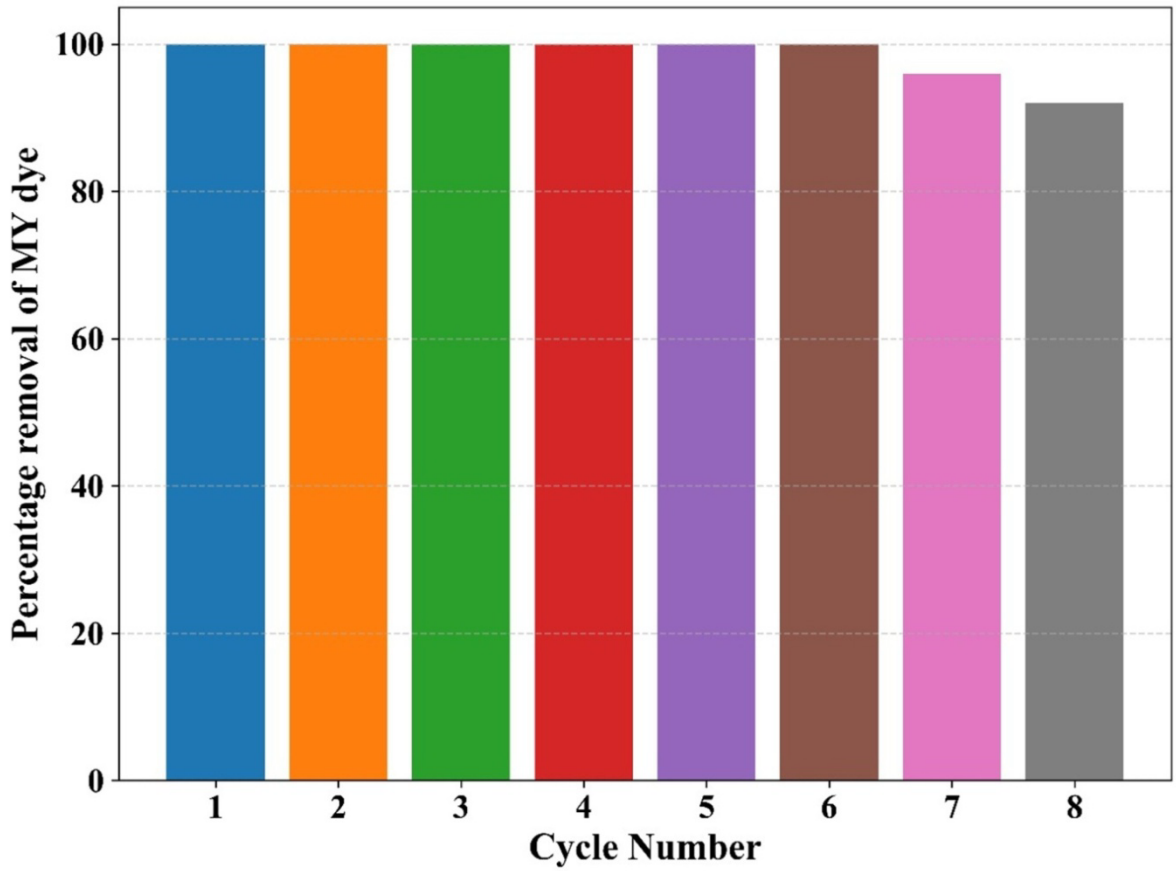

Figure .9 Degradation efficiency of(Fe, S)-codopedTiO_2

Chemical Oxygen Demand (COD) Analysis

The synthesized (Cu, N)-codoped TiO_2 photocatalyst has shown excellent potential for wastewater treatment by successfully reducing the chemical oxygen demand (COD) of My dye solution[62]. In this present study, COD of My dye solution was measured before and after the photocatalytic degradation. Initially, the COD was approximately 15,468 mg/L. After treatment with (Fe, S)-codoped TiO_2 photocatalyst under sunlight irradiation for 30 minutes, the COD was drastically reduced to 30mg/L, indicating nearly complete mineralization of the dye molecules and effective removal of color from the solution[27]. These findings demonstrate the excellent degradation efficiency of organic contaminants by the synthesized (Fe, S)-codoped TiO_2 photocatalyst, indicating a possible solution for wastewater treatment.

Total Organic Carbon Analysis

To evaluate the mineralization of organic pollutants and their degradation products during the photocatalytic process, total organic carbon (TOC) analysis was analyzed before and after the photocatalytic degradation ofthe MY dye solution [28]. The organic carbon content was significantly, indicating the effective breakdown of the organic components showing 98.66 % removal efficiency. These results confirm that the synthesized (Fe, S)-codoped TiO_2photocatalystis highly effective in rapidly degrading the toxic organic pollutants in water.

CONCLUSION

In the present study, undoped TiO_2 and(Fe,S) co-doped TiO_2 photocatalysts were successfully synthesized and systematically characterized using various analytical and spectroscopic techniques. XRD

analysis confirmed that Fe–S co-doping did not alter the intrinsic tetragonal anatase phase of TiO_2, and no secondary impurity phases were detected, indicating successful incorporation of dopants into the TiO_2 lattice. SEM analysis revealed that Fe–S co-doped TiO_2 exhibited uniformly distributed nanoparticles with slight agglomeration, suggesting homogeneous dispersion of Fe and S ions on the TiO_2 surface. EDX analysis further confirmed the presence of Fe and S elements without impurities, validating the effectiveness of the co-doping process. TEM analysis showed that both undoped and (Fe,S) co-doped TiO_2 nanoparticles possessed predominantly spherical morphology with good crystallinity, which is favorable for photocatalytic applications. UV–visible diffuse reflectance studies demonstrated a significant reduction in band gap energy of TiO_2 upon Fe–S co-doping, resulting in enhanced visible-light absorption. The (Fe,S) co-doped TiO_2 photocatalyst exhibited superior photocatalytic degradation efficiency toward organic dye pollutants under sunlight irradiation compared to undoped TiO_2. Kinetic studies followed the Langmuir–Hinshelwood model, indicating pseudo-first-order reaction behavior. The effective mineralization of the dye was further supported by notable reductions in COD and TOC values. Additionally, the(Fe,S) co-doped TiO_2 photocatalyst showed excellent stability and reusability over multiple cycles without significant loss of activity. Overall, the results confirm that (Fe,S) co-doping is an efficient strategy to enhance the visible-light-driven photocatalytic performance of TiO_2, making it a promising material for environmental remediation applications.

ACKNOWLEDGEMENT

The authors are thankful to Noorul Islam Institute of Technology and Science, Coimbatore, India; Abdul Kalam Research Centre, Sacred Heart College (Autonomous), Tirupattur District, India; and Alagappa University, Karaikudi, India, for providing the necessary resources and support for this work.

CONFLICT OF INTEREST

The authors declare no conflict of interest.

REFERENCES

[1] EK, K.V., 2023. Solar light driven transition metal codopedZnO (Ag, Ni-codopedZnO) photocatalyst for environmental remediation. *Indian Journal of Chemical Technology (IJCT)*, *30*(3), pp.352-360.

[2]Uribe-López, M.C., Hidalgo-López, M.C., López-González, R., Frías-Márquez, D.M., Núñez-Nogueira, G., Hernández-Castillo, D. and Alvarez-Lemus, M.A., 2021. Photocatalytic activity of ZnO nanoparticles and the role of the synthesis method on their physical and chemical properties. *Journal of Photochemistry and photobiology A: Chemistry*, *404*, p.112866.

[3]Anucha, C.B., Altin, I., Bacaksiz, E. and Stathopoulos, V.N., 2022. Titanium dioxide (TiO_2)-based photocatalyst materials activity enhancement for contaminants of emerging concern (CECs) degradation: In the light of modification strategies. *Chemical Engineering Journal Advances*, *10*, p.100262.

[4]Sibhatu, A.K., Weldegebrieal, G.K., Sagadevan, S., Tran, N.N. and Hessel, V., 2022. Photocatalytic activity of CuO nanoparticles for organic and inorganic pollutants removal in wastewater remediation. *Chemosphere*, *300*, p.134623.

[5]Saini, S., Kaur, M., Pahwa, C. and Singh, S., 2024. Temperature Dependent Structural, Optical, Photocatalytic and Magnetic Properties of WO3 Nanoparticles. *Journal of Water and Environmental Nanotechnology*, *9*(3), pp.318-326.

[6]Jayaraj, S.K., Sadishkumar, V., Arun, T. and Thangadurai, P., 2018. Enhanced photocatalytic activity of V2O5 nanorods for the photodegradation of organic dyes: a detailed understanding of the mechanism and their antibacterial activity. *Materials Science in Semiconductor Processing*, *85*, pp.122-133.

[7]Basahel, S.N., Ali, T.T., Mokhtar, M. and Narasimharao, K., 2015. Influence of crystal structure of nanosized ZrO2 on photocatalytic degradation of methyl orange. *Nanoscale research letters*, *10*(1), p.73.
[8]Ezeibe Anderson, U., Nleonu Emmanuel, C., Onyemenonu Christopher, C. and Arrousse Nadia, N.C.C., 2022. Photocatalytic activity of aluminium oxide nanoparticles on degradation of ciprofloxacin. *Saudi J Eng Technol*, *7*(3), pp.132-136.
[9]Kim, S.P., Choi, M.Y. and Choi, H.C., 2016. Photocatalytic activity of SnO2 nanoparticles in methylene blue degradation. *Materials Research Bulletin*, *74*, pp.85-89.
[10]Duraisamy, N., Kandiah, K., Rajendran, R., S, P., R, R. and Dhanaraj, G., 2018. Electrochemical and photocatalytic investigation of nickel oxide for energy storage and wastewater treatment. *Research on Chemical Intermediates*, *44*(9), pp.5653-5667.
[11]Silva-Osuna, E.R., Vilchis-Nestor, A.R., Villarreal-Sanchez, R.C., Castro-Beltran, A. and Luque, P.A., 2022. Study of the optical properties of TiO2 semiconductor nanoparticles synthesized using Salvia rosmarinus and its effect on photocatalytic activity. *Optical Materials*, *124*, p.112039.
[12] Basavarajappa, P.S., Patil, S.B., Ganganagappa, N., Reddy, K.R., Raghu, A.V. and Reddy, C.V., 2020. Recent progress in metal-doped TiO2, non-metal doped/codoped TiO2 and TiO2 nanostructured hybrids for enhanced photocatalysis. *International journal of hydrogen energy*, *45*(13), pp.7764-7778.
[13]Fatima, R., Kadhem, A.A., Sajjad, A., Noman, H.M., Kiran, K.S., Kumar, S., Sunitha, S., Ray, S., Sariyevich, X.X., Fozil, X. and Shahid, M., 2023. Optimized Cu/Zr Co-doped TiO2 nanocomposites as high performance photocatalyst for visible light induced methylene blue degradation. *Journal of Alloys and Compounds*, p.184031.
[14] Yitagesu, G.B., Leku, D.T., Seyume, A.M., Workneh, G.A., 2024. Synthesis of TiO_2/CuO and its application for the photocatalytic removal of the methylene blue dye. *ACS Omega*, **9**(36), 39398126. https://doi.org/10.1021/acsomega.4c03472
[15] Sirivallop, A., Areerob, T. and Chiarakorn, S., 2020. Enhanced visible light photocatalytic activity of N and Ag doped and co-doped TiO2 synthesized by using an in-situ solvothermal method for gas phase ammonia removal. *Catalysts*, *10*(2), p.251.
[16]Faustino, E., da Silva, T.F., Cunha, R.F., Guelfi, D.R.V., Cavalheri, P.S., de Oliveira, S.C., Caires, A.R.L., Casagrande, G.A., Cavalcante, R.P. and Junior, A.M., 2022. Synthesis and characterization of N and Fe-doped TiO2 nanoparticles for 2, 4-Dimethylaniline mineralization. *Nanomaterials*, *12*(15), p.2538.
[17] Zhao, Z., Omer, A.A., Qin, Z., Osman, S., Xia, L. and Singh, R.P., 2020. Cu/N-codoped TiO2 prepared by the sol-gel method for phenanthrene removal under visible light irradiation. *Environmental Science and Pollution Research*, *27*(15), pp.17530-17540.
[18]Jaiswal, R., Bharambe, J., Patel, N., Dashora, A., Kothari, D.C. and Miotello, A., 2015. Copper and Nitrogen co-doped TiO2 photocatalyst with enhanced optical absorption and catalytic activity. *Applied Catalysis B: Environmental*, *168*, pp.333-341.
[19]Isari, A.A., Hayati, F., Kakavandi, B., Rostami, M., Motevassel, M. and Dehghanifard, E., 2020. N, Cu co-doped TiO2@ functionalized SWCNT photocatalyst coupled with ultrasound and visible-light: an effective sono-photocatalysis process for pharmaceutical wastewaters treatment. *Chemical Engineering Journal*, *392*, p.123685.
[20]Choi, J., Park, H. and Hoffmann, M.R., 2010. Effects of single metal-ion doping on the visible-light photoreactivity of TiO2. *The Journal of Physical Chemistry C*, *114*(2), pp.783-792.
[21]Shannon, R.D., 1976. Revised effective ionic radii and systematic studies of interatomic distances in halides and chalcogenides. *Foundations of Crystallography*, *32*(5), pp.751-767.

[22]Lin, Y.H., Hsueh, H.T., Chang, C.W. and Chu, H., 2016. The visible light-driven photodegradation of dimethyl sulfide on S-doped TiO2: Characterization, kinetics, and reaction pathways. *Applied Catalysis B: Environmental*, *199*, pp.1-10.
[23]Wu, M., Yang, B., Lv, Y., Fu, Z., Xu, J., Guo, T. and Zhao, Y., 2010. Efficient one-pot synthesis of Ag nanoparticles loaded on N-doped multiphase TiO2 hollow nanorod arrays with enhanced photocatalytic activity. *Applied Surface Science*, *256*(23), pp.7125-7130.
[24]Jeyachitra, R., Kalpana, S., Senthil, T.S. and Kang, M., 2020. Electrical behavior and enhanced photocatalytic activity of (Ag, Ni) co-doped ZnO nanoparticles synthesized from co-precipitation technique. Water Science and Technology, 81(6), pp.1296-1307.
[25] Thongpool, V., Phunpueok, A., Jaiyen, S. and Sornkwan, T., 2020. Synthesis and photocatalytic activity of copper and nitrogen co-doped titanium dioxide nanoparticles. *Results in Physics*, *16*, p.102948.
[26] Ahmadiasl, R., Moussavi, G., Shekoohiyan, S. and Razavian, F., 2022. Synthesis of Cu-doped TiO2 nanocatalyst for the enhanced photocatalytic degradation and mineralization of gabapentin under UVA/LED irradiation: characterization and photocatalytic activity. *Catalysts*, *12*(11), p.1310.
[27]Lian, P., Qin, A., Liu, Z., Ma, H., Liao, L., Zhang, K. and Li, N., 2023. Facile synthesis to porous TiO2 nanostructures at low temperature for efficient visible-light degradation of tetracycline. *Nanomaterials*, *14*(11), p.943.
[28]León, A., Reuquen, P., Garín, C., Segura, R., Vargas, P., Zapata, P. and Orihuela, P.A., 2017. FTIR and Raman characterization of TiO2 nanoparticles coated with polyethylene glycol as carrier for 2-methoxyestradiol. *Applied Sciences*, *7*(1), p.49.